Comparative study of Minnesota functionals performance on ferroelectric BaTiO₃ and PbTiO₃

Maggie Kingsland,[1] K. A. Lynch,[1] S. Lisenkov,[1,*] Xiao He,[2] and I. Ponomareva[1]

[1]*Department of Physics, University of South Florida, Tampa, Florida 33620, USA*
[2]*Shanghai Engineering Research Center of Molecular Therapeutics and New Drug Development,*
School of Chemistry and Molecular Engineering, East China Normal University, Shanghai 200062, China

Density-functional-theory-based simulations are the leading tool for the computational investigation of ferroelectrics and the parametrization of their classical potentials. However, the predictions often depend strongly on the exchange-correlation functional. The most popular choices, the LDA and GGA, tend to underestimate or overestimate some structural, electric, and energy properties. These impede the development of highly accurate classical potentials that extend the reach of first-principles simulations to finite temperatures and realistic sizes. In this work, we investigate the performance of recently developed Minnesota exchange-correlation functionals on the prototypical ferroelectrics BaTiO₃ and PbTiO₃ in comparison with some popular ones. We find that there exists a strong correlation between predictions for some properties (tetragonality, phase energy difference, and polarization) by different functionals. Along the correlation line, we find a range of functionals (including some from the Minnesota suite) whose predictions fall between those of the LDA and those of the GGA and, therefore, offer an improvement. A way to relatively rank functional performance with respect to chosen benchmarks is proposed and applied to identify the top performers for BaTiO₃ and PbTiO₃. The performance is found to be material dependent. Therefore, we propose that the performance assessment carried out in this work is employed to "screen" functionals prior to their use on ferroelectrics. Quick and computationally inexpensive, it is likely to lead to improved descriptions, especially for classical potential parametrization. The Minnesota functional suite is found to be suitable for this task.

I. INTRODUCTION

Ferroelectrics are materials that possess spontaneous polarization that is reversible by the application of an electric field. They find numerous applications in capacitors, FeRAM, piezoelectric devices, and RFID chips. Density functional theory (DFT) has been an indispensable tool to computationally study ferroelectric perovskites. It also has been successfully used to develop classical potentials for ferroelectrics that extend the reach of computations to finite temperatures and realistic sizes. However, one of the long-standing issues with the latter computations has been the inability of many such potentials to quantitatively describe the temperature evolution of ferroelectric properties. One important example is the failure to correctly capture the Curie temperature in such simulations. Specifically, local density approximation (LDA)–based parametrizations underestimate the Curie temperatures of these materials [1–9], and the generalized gradient approximation Perdew-Burke-Ernzerhof (GGA PBE) functional overestimates it [1,2,5–9]. Consequently, the outstanding question is which functional(s) is(are) the most appropriate to study structural, electric, and energetic properties of ferroelectrics so that accurate classical force fields can be developed. Note, that we list all acronyms for the exchange-correlation functionals in Table VI of the Appendix.

Recently, this question was addressed for three functionals (LDA, GGA, and SCAN meta-GGA) in Ref. [10]. It was shown that the SCAN functional significantly improves upon the traditional LDA/GGA for structural, electric, and energetic properties of diversely bonded ferroelectric materials. A preceding study [2] investigated the performance of the LDA, PBE, HSE, SCAN, and B1WC on BaTiO₃ (BTO), PbTiO₃ (PTO), and BiFeO₃. In particular, the electrical, structural, and energetic properties were studied. It was found that SCAN predicts these properties within the closest agreement of the computationally expensive B1WC hybrid functional [8] that has been designed specifically for ferroelectrics. In Ref. [11], it was found that the van der Waals density functional with C09 exchange demonstrated superior performance on PTO, BTO, and KNO₃ compared with the LDA, PBE, and PBEsol. The role of the energy functional in interatomic interactions accuracy in the effective Hamiltonian for predicting ferroelectric phase transitions in perovskite oxides was discussed in Ref. [9]. Eight perovskite oxides including PTO and BTO were investigated, and it was concluded that the SCAN offers a significant improvement of lattice constants compared to earlier LDA results. Consequently, the prediction of Curie temperatures from the effective Hamiltonian derived using the SCAN functional improved in comparison to the LDA-based one. However, it was found that the T_C for BTO was still significantly underestimated, while underestimation was less severe for PTO and KNO₃. In Ref. [12], strained and stress-free tetragonal BTO was investigated using the full range of exchange-correlation functionals. It was found that

*slisenk@usf.edu

for unstrained BTO the best estimates for the spontaneous polarization and tetragonality are given by the PBEsol, TPSS, TPSS + U, HSEsol, and B1-WC(PP).

Recently, the new set of the so-called Minnesota functionals (GAM, HLE17, revM06-L, MN12-L, MN15-L, N12, N12-SX, SOGGA, SOGGA11, SOGGA11-X) was introduced [13] and some have been implemented in the VASP DFT simulation package [14–17], which is one popular tool for study of ferroelectrics. Only a few of these functionals have been applied to the study of ferroelectrics. In Ref. [18], the cubic and tetragonal lattice constants of PTO were reported for the SOGGA, M06-L, PBEsol, TPSS, and PBE. The SOGGA was shown to better predict the lattice constants than the others. In Ref. [19], the SOGGA functional was found to perform well in predicting structural and vibrational properties of PTO and PbZrO$_3$ in comparison to experiment. In Ref. [20], PTO's cubic and tetragonal lattice constants have been reported for the LDA, PBE, PBEsol, TPSS, SOGGA, M06L, SCAN, and TM; however, the focus was the performance of the TM functional in comparison with others. The goal of this paper is to assess the performance of these newly introduced functionals in comparison with some of the traditional ones (LDA, PBE, PBEsol, AM05, SCAN, HSE06) for studies of the prototypical ferroelectrics PTO and BTO. The paper is organized as follows: In Sec. II, we provide a brief overview of the functionals utilized in the study. In Sec. III, we describe the computational methodology, while Secs. IV and V are dedicated to the Results and Discussion, respectively. We provide conclusions in Sec. VI.

II. BASIC DESCRIPTION OF THE FUNCTIONALS

An excellent review of density functionals is available in Ref. [21]. To briefly introduce the functionals used in the study, we adapt Perdew's metaphorical Jacob's Ladder [21] (see Fig. 1). In the first rung of the ladder, we find the LDA, which is the simplest exchange-correlation functional that depends only on the electron density [21]. In the second rung of the ladder is the GGA functional, which improves upon the systematic errors of the LDA by accounting for inhomogeneities in the density through the incorporation of a density gradient. Perhaps, the most popular representative of this type of functional is the PBE. In the same rung, we find the so-called nonseparable gradient approximation (NGA) functionals. They differ from the GGA in that they use one additional variable that depends only on the density [21]. The particular representatives of this class considered here are the N12 and GAM. To further improve the accuracy of the functionals, the second derivative information can be included through the Laplacian of the density or the kinetic energy density [21]. Such functionals define the third rung of Jacob's Ladder and are known as the meta-GGA (or meta-NGA). In this study, we consider five representatives which are shown in Fig. 1. However, there exist limitations of the exchange-correlation functionals that cannot be remedied by the inclusion of local ingredients [21]. The self-interaction error is one such limitation. One way to overcome this is to combine the exact exchange and density functionals which give origin to the hybrid functionals. These occupy the fourth rung of Jacob's Ladder and are termed the hybrid (meta)GGA/(meta)NGA. The
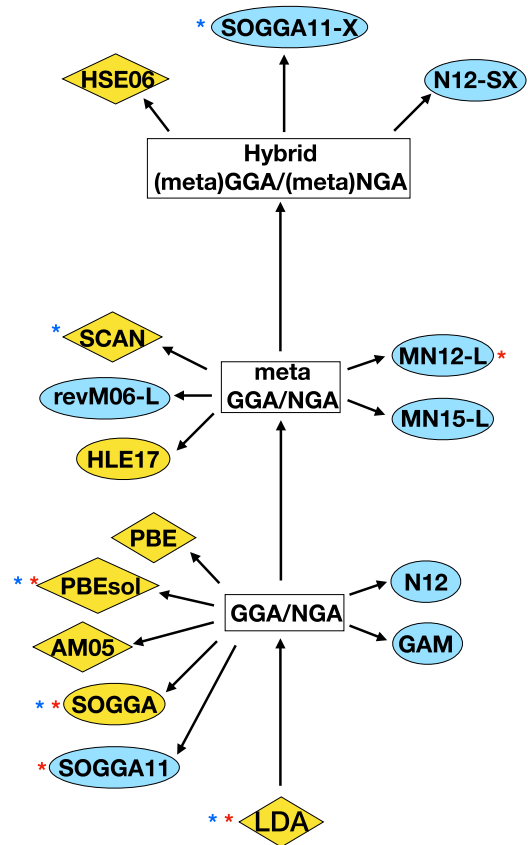

FIG. 1. Jacob's Ladder diagram describing the functionals that are investigated in this work. The functionals in diamonds are the standard representative(s) in each rung, while those in ovals are the Minnesota ones. Yellow shading indicates functionals that have been previously used on ferroelectrics, while blue shading indicates those that have not been tested. Blue (red) asterisks denote the best-performing functionals found in this study for the case of BTO (PTO), respectively.

representatives considered in this study are also shown in Fig. 1. In addition, we also include the hybrid HSE06 [22] functional for comparison purposes within the hybrid rung. Note that the HSE differs from the standard or meta-GGA/NGAs due to its inclusion of fractional Hartree-Fock (HF) exchange parameters which describe nonlocality [22–24]. We next provide a brief description of the Minnesota functionals [13] which we chose for this investigation.

A. GGA/NGA functionals

The second-order generalized gradient approximation (SOGGA) expands upon the GGA, making it exact through the gradient expansion's second order for the exchange and correlation energies [18]. It was originally developed to fix the exchange and correlation potentials that are neglected in the GGAs [18]. In the initial paper, the SOGGA was shown to better estimate the lattice constants than other GGAs, such as the PBE [18]. There have been recent studies that indicate that the SOGGA estimates the cubic lattice constant, tetragonality, and ferroelectric properties of PTO well [18–20]. Reference [18] reports that SOGGA's estimation of lattice constants (for

both the cubic and the tetragonal phases) for PTO are closer to experimental results than the lattice constants found by the PBE. Reference [19] describes the potential for the SOGGA to correctly describe the vibrational frequencies of PZO and PTO. It also finds that the nonzero temperature lattice vectors are well predicted by the SOGGA. The SOGGA11 was created to update the SOGGA functional to make it more accurate for predicting molecular energies [25]. It also was shown to be accurate when predicting molecular bond lengths [25]. To our knowledge, there have been no previous publications about SOGGA11's performance on ferroelectrics. The parameterized exchange-correlation functional N12 uses the NGA and was developed to more accurately predict the lattice constants and bond lengths without losing the accuracy of cohesive and atomization energies [26]. It is dependent on the spin-labeled electron densities and their reduced gradient [26]. The N12 was shown to be better at estimating the cohesive energy, atomization energy, lattice constants, and bond lengths than other similar functionals when tested using various databases [26]. We are not aware of any previous works that directly test this functional on PTO and/or BTO. The gradient approximation for molecules (GAM) is an NGA functional that was developed to be excellent at estimating barrier heights at the expense of less accurate lattice constants [27]. In general, the lattice constants are approximately twice as incorrect as the PBE and roughly three times as inaccurate as the HSE06. However, the GAM still estimated reasonable results of the lattice constants for semiconductors [27].

B. Meta-GGA/NGA functionals

The local exchange-correlation functional MN12-L is based on the N12 such that it is an NGA but it also includes the kinetic energy density contribution, which is not found in the N12 [28]. It was shown to be more accurate than other local functionals in terms of cohesive energies and other such properties [28] but was average at estimating semiconductor lattice constants [28]. Similar to the MN12-L is the MN15-L, which has the same mathematical construction as the MN12-L but is optimized using a larger database [29]. It was shown to give reasonably accurate results across the board when tested on a large variety of databases compared to other functionals [29]. To our knowledge, there are no previous studies on the performance of either the MN12-L or the MN15-L on ferroelectrics. Recently, the High Local Exchange 2017 (HLE17) functional was developed [30], with the goal of better predicting bandgap energies for semiconductors and molecular excitation energies [30]. It was noted that the HLE17 tends to underestimate the lattice constants, worse so than the HSE06 but still better than the PBE and GAM [30]. A previous study investigated HLE17's performance on five perovskites, including $SrTiO_3$ and $CaTiO_3$, and showed that it gave a better estimation of bandgaps than the PBE functionals, almost comparable to the HSE06 [31]. We are not aware of any previous publications on BTO or PTO using the HLE17. The final functional we highlight in this category is the revised M06 (revM06-L) functional, which is an improved version of the Minnesota 2006 local functional (M06-L). The M06-L is a local meta-GGA and has proven to be accurate for a broad range of chemical properties, such as noncovalent interactions, bond

TABLE I. References for some of the studies of prototypical ferroelectric perovskites using different functionals.

Functional	Tested on ferroelectrics
LDA [35,36]	BTO [1,2], PTO [1,2]
PBE [37,38]	BTO [1,2], PTO [1,2]
PBEsol [39]	BTO [11,12,40], PTO [11,18,20,40,41]
AM05 [42,43]	PTO [41]
SCAN [1,2,10]	BTO [1,2], PTO [1,2]
HSE06 [22–24]	BTO [1,2], PTO [1,2]
GAM [27]	Not tested on ferroelectrics
HLE17 [30,31]	$SrTiO_3$, $CaTiO_3$ [31]
revM06-L [32]	Not tested on ferroelectrics
MN12-L [28]	Not tested on ferroelectrics
MN15-L [29]	Not tested on ferroelectrics
N12 [26]	Not tested on ferroelectrics
N12-SX [34]	Not tested on ferroelectrics
SOGGA [18]	PTO [18–20]
SOGGA11 [25]	Not tested on ferroelectrics
SOGGA11-X [33]	Not tested on ferroelectrics

lengths, and vibrational frequencies [32]. It was revised and trained against a larger set of databases in order to enhance its accuracy [32]. The revM06-L functional was shown to be a better predictor of bandgap energies compared to the MN15-L, GAM, and PBE but was worse than the HSE06 [32]. This functional appears promising for testing on ferroelectrics and has not been investigated to our knowledge.

C. Hybrids

The SOGGA11-X is the global hybrid functional extension of the SOGGA11 and was reported to have a better overall performance than other global hybrid GGAs at the time it was introduced [33]. In Ref. [33], the SOGGA11-X shows better estimations of barrier heights, alkyl-bond dissociation energies, and noncovalent interactions. The N12-SX functional is an extension of the N12 functional into a hybrid functional such that it now contains a percentage of the short-range Hartree-Fock (HF) exchange and is screened in long-range HF exchange [34]. It is the same as the N12 in that it depends on the density and density gradient [34]. The N12-SX was shown to estimate solid-state physical properties more accurately than the HSE06 when tested on various semiconductor databases in addition to other databases [34]. To our knowledge, there have been no previous studies of SOGGA11-X's or N12-SX's performance on ferroelectrics. It should be noted that hybrid functionals come at a much greater computational cost than nonhybrid ones.

Table I compiles some references available from the literature on studies of prototypical ferroelectric perovskites using the aforementioned functionals. It reveals that many of them have not been previously studied on ferroelectrics so our study fills these gaps.

III. METHODOLOGY

To achieve our goal, we tested selected Minnesota functionals (GAM, HLE17, revM06-L, MN12-L, MN15-L, N12,
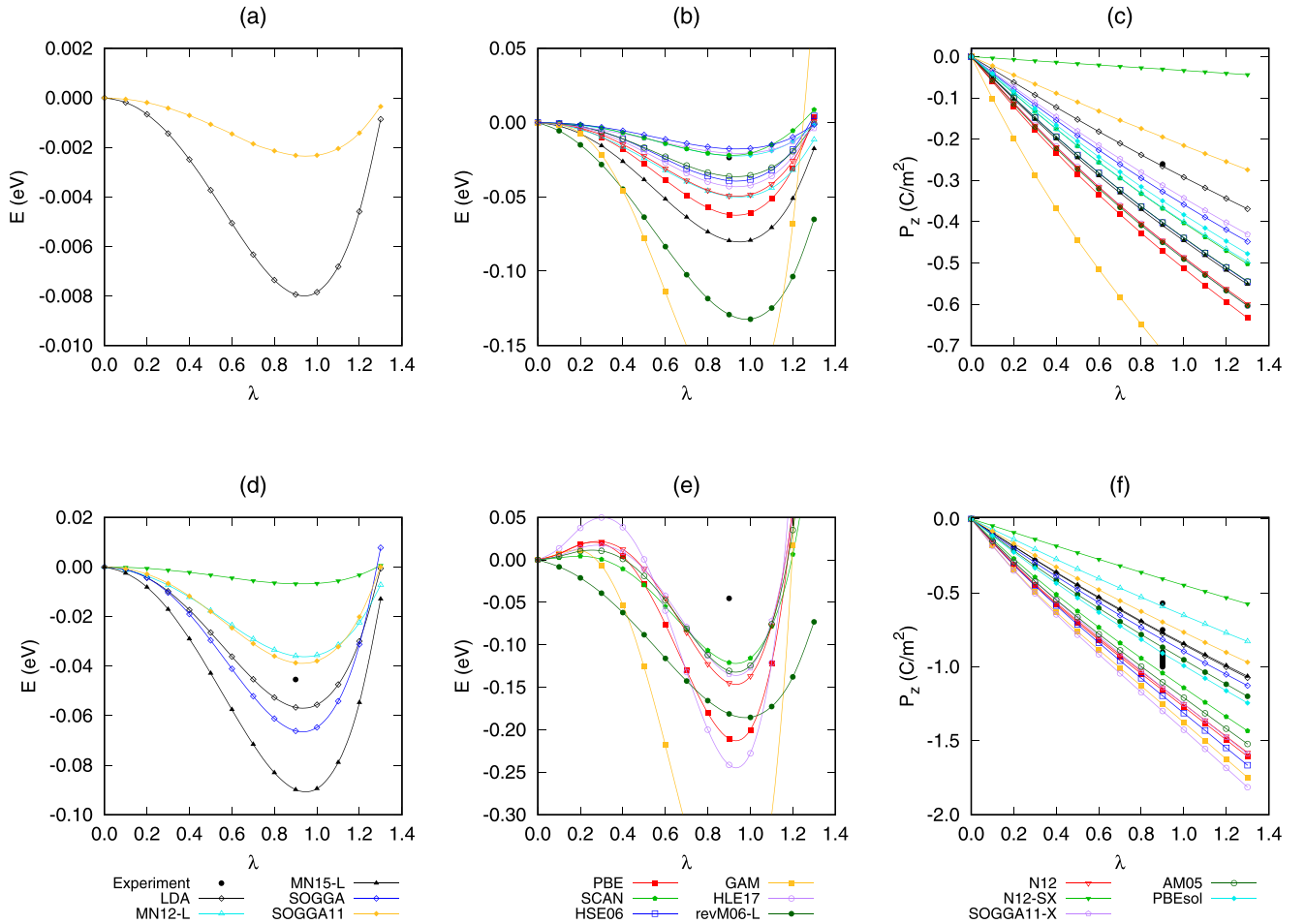
FIG. 2. Energy (a, b, d, e) and polarization (c, f) along the distortion path for BTO and PTO, respectively. Shallow energy wells (a, d); deeper wells (b, e). Experimental data for BTO are taken from Refs. [1], [2], [50], and [52]. Experimental data for PTO are taken from from Refs. [1], [50], [55], and [56]. Note that the GAM data are outside of plotting range.

N12-SX, SOGGA, SOGGA11, SOGGA11-X), which are available upon request from Dr. Donald Truhlar and coauthors [13], on the prototypical ferroelectrics PTO and BTO. We decided to focus on the tetragonal and cubic phases of these materials since these are common for both materials. For our DFT simulations, we used the VASP software with the projector-augmented wave method [14–17]. Semicore s states are taken as valence states for Ba and Ti; semicore d states are taken as valence states for Pb. We use a Γ-centered $8 \times 8 \times 8$ k-point mesh and an energy cutoff of 900 eV for all calculations. The initial structures for both cubic and tetragonal phases of both BTO and PTO were downloaded from the Materials Research Project [44,45] and then fully relaxed using each functional until forces on atoms were less than 1 meV/Å. These computational parameters are in line with Ref. [46], which provides accurate results. Next, we used the ISOTROPY software [47,48] to construct the distortion path between the cubic and the tetragonal phases. The distortion parameter λ is equal to 0 for the cubic phase and to 0.9 for the teragonal phase. We simulated 14 steps along the distortion path between $\lambda = 0$ and $\lambda = 1.3$. The energy and polarization were calculated along the distortion path. An example of the energy and polarization evolution along the distortion path is shown in Figs. 2(a)–2(c) for BTO. We have

also computed the bandgaps for BTO and PTO structures, using the postprocessing utility VASPKIT [49].

IV. RESULTS

We begin by listing the computational data for BTO and PTO in Tables II and III, respectively. The tables report the cubic lattice constant a_c, tetragonality c/a, absolute value of spontaneous polarization P_s, and difference in the energy ΔE between the cubic and the tetragonal phases. These properties are paramount in the description of ferroelectrics. We also have included the value for the bandgap energies in the tables. It should be noted that most of the experimental values are at room temperature, while simulations correspond to 0 K. There are no experimental measurements for the ΔE so it is customary (Refs. [1] and [50]) to use the transition temperature to estimate this value. At the transition temperature, the free energies of the cubic and tetragonal phases are equal. Thus, the difference in the energies is proportional to the entropy difference between the two phases, which we estimate on the basis of the two-state spin model where each perovskite unit cell has a "spin" (dipole moment). Within the model, a completely disordered paraelectric phase will have a $k_B T \ln 2^N$ entropic term in the free energy, while for

TABLE II. Computational data for BTO: cubic lattice constant a_c, tetragonality c/a, spontaneous polarization P_s, energy difference between the tetragonal and the cubic phase ΔE, and bandgap E_g in the tetragonal phase. Experimental values (Expt) for the same properties are listed in the last row. For each property, we list the computed value, percentage error with respect to the experimental value, and rank of the functional. The reported experimental bandgap energy is an average of the experimental values.

	a_c (Å)			c/a			P_s ($\frac{\mu C}{cm^2}$)			ΔE ($\frac{meV}{f.u.}$)			E_g (eV)			Rank
	Value	Error	Rank	Value	Error	Rank	Value	Error	Rank	Value	Error	Rank	Value	Error	Rank	
PBEsol	3.98	−0.1	2	1.026	1.6	6	35.0	34.5	5	22.3	−5.2	1	2.0	−38.9	7–9	1
SOGGA	3.98	−0.3	4	1.021	1.1	4	32.7	25.8	3	17.6	−25.1	4	2.0	−38.9	7–9	2
SOGGA11X	3.97	−0.5	7	1.024	1.4	5	31.2	19.9	2	20.5	−12.6	3	5.2	57.5	16	3
LDA	3.95	−0.9	11	1.013	0.3	1–2	26.6	2.1	1	7.9	−66.2	6	2.0	−39.2	10	4
SCAN	4.00	0.4	6	1.031	2.1	7	36.8	41.5	7	22.0	−6.4	2	2.0	−38.6	6	5
SOGGA11	3.96	−0.7	8–9	1.007	−0.3	1–2	17.1	−34.2	4	2.3	−90.1	9	2.0	−41.4	14–15	6–7
AM05	3.99	0.1	1	1.036	2.6	9	40.2	54.5	8	36.1	53.7	5	2.0	−38.9	7–9	6–7
HSE06	3.99	0.2	3	1.043	3.3	12	40.2	54.6	9	39.1	66.2	7	3.0	−8.8	2	8
MN12-L	4.01	0.7	8–9	1.033	2.3	8	36.6	40.9	6	49.5	110.8	12	2.4	−27.5	3	9
N12	3.97	−0.3	5	1.046	3.6	14	44.6	71.5	11	49.2	109.4	11	2.0	−40.2	12	10
N12-SX	4.10	2.9	16	1.000	−1.0	3	3.0	−88.3	15	0.1	−99.7	10	3.6	−7.3	1	11
HLE17	3.89	−2.5	15	1.040	3.0	11	44.7	72.0	12	42.8	82.3	8	2.0	−41.4	14–15	12
MN15-L	4.07	2.0	14	1.040	3.0	10	40.9	57.4	10	79.5	238.1	14	2.3	−31.4	4	13
revM06-L	4.02	0.9	10	1.043	3.3	13	45.0	73.2	13	129.1	449.5	15	2.1	−5.6	5	14
PBE	4.03	1.2	12	1.058	4.7	15	47.1	81.3	14	61.9	163.6	13	2.0	−39.8	11	15
GAM	4.06	1.7	13	1.152	14.0	16	71.2	173.9	16	198.3	744.0	16	2.0	−40.5	13	16
Expt	33.986	(294 K)	[51]	1.010	(294 K)	[51]	26	(298 K)	[1,52]	23.5	(393 K)	[50]	3.325	(294 K)	[53]	–

the completely ordered tetragonal phase this term is 0 since there is just one possible configuration. Here N is the total number of spins (or unit cells). Strictly speaking, there are two configurations to account for two possible directions of polarization but this can be ignored in comparison with the 2^N contribution. Then $\Delta E = k_B T_C \ln 2$ per unit cell estimates the

depth of the tetragonal well. It should be noted that for BTO the ground state is rhombohedral. Nevertheless, we still use the same expression to estimate T_C, as at this temperature the ferroelectric undergoes the transition from tetragonal to cubic phase. For each property, we calculate the error with respect to the experimental value listed in the last row and report it as

TABLE III. Computational data for PTO: cubic lattice constant a_c, tetragonality c/a, spontaneous polarization P_s, energy difference between the tetragonal and the cubic phase ΔE, and bandgap E_g in the tetragonal phase. Experimental values (Expt) for the same properties are listed in the last complete row. For each property, we list the computed value, percentage error with respect to the experimental value, and rank of the functional.

|	a_c (Å)			c/a			P_s ($\frac{\mu C}{cm^2}$)			ΔE ($\frac{meV}{f.u.}$)			E_g (eV)			Rank
	Value	Error	Rank	Value	Error	Rank	Value	Error	Rank	Value	Error	Rank	Value	Error	Rank	
LDA	3.89	0.2	1	1.044	−2.5	5	77.5	3.4	1	56.7	24.9	3	1.9	−48.3	16	1
SOGGA11	3.90	0.4	2	1.036	−3.3	6	69.6	−7.2	3	38.7	−14.7	1	1.9	−47.8	14–15	2
SOGGA	3.91	0.8	5	1.058	−1.2	2	83.2	10.9	4	66.2	45.7	4	1.9	−46.1	13	3
PBEsol	3.92	1.1	6–7	1.085	1.3	3	93.5	24.7	7	84.1	85.2	6	2.0	−44.7	12	4
MN12-L	3.94	1.6	14	1.029	−3.9	7	59.1	−21.2	6	36.0	−20.8	2	2.4	−32.8	3	5
MN15-L	3.99	2.9	14	1.049	−2.0	4	78.0	4.0	2	89.9	97.9	7	2.3	−35.3	4	6
revM06-L	3.95	1.8	12	1.069	−0.2	1	86.1	14.8	5	181.3	299.4	13	2.0	−43.9	11	7
SCAN	3.93	1.4	9	1.142	6.7	9	104.2	39.0	8	120.8	166.1	8	2.1	−41.9	7	8–9
SOGGA11-X	3.90	0.5	3	1.175	9.7	10	113.9	51.9	11	134.3	195.8	10	5.2	43.2	10	8–9
N12-SX	4.04	4.2	16	1.013	−5.4	8	40.5	−46.1	9	6.8	−85.1	5	3.2	−10.7	1	10–11
AM05	3.92	1.1	8	1.177	9.9	11	110.4	47.2	10	130.7	187.8	9	2.1	−42.5	8–9	10–11
N12	3.91	0.8	4	1.200	12.1	12	114.2	52.3	12	144.9	219.2	11	2.1	−42.5	8–9	12
HSE06	3.92	1.1	6–7	1.212	13.2	13	119.5	59.4	14	169.5	273.4	12	2.9	−20.0	2	13
PBE	3.97	2.3	13	1.230	14.9	14	115.8	54.4	13	210.5	363.7	14	2.2	−38.9	6	14
HLE17	3.82	−1.5	10	1.252	16.9	15	129.8	73.1	16	241.4	431.7	15	1.9	−47.8	14–15	15
GAM	3.99	2.9	15	1.285	20.0	16	125.3	67.0	15	456.1	904.6	16	2.3	−36.4	5	16
Expt	3.88	(0 K)	[1,54]	1.071	(0 K)	[1,54]	57	(297 K)	[1]	45.4	(760 K)	[50]	3.6	(294 K)	[55]	–
							75	(293 K)	[50]							
							90–100	(293 K)	[56]							
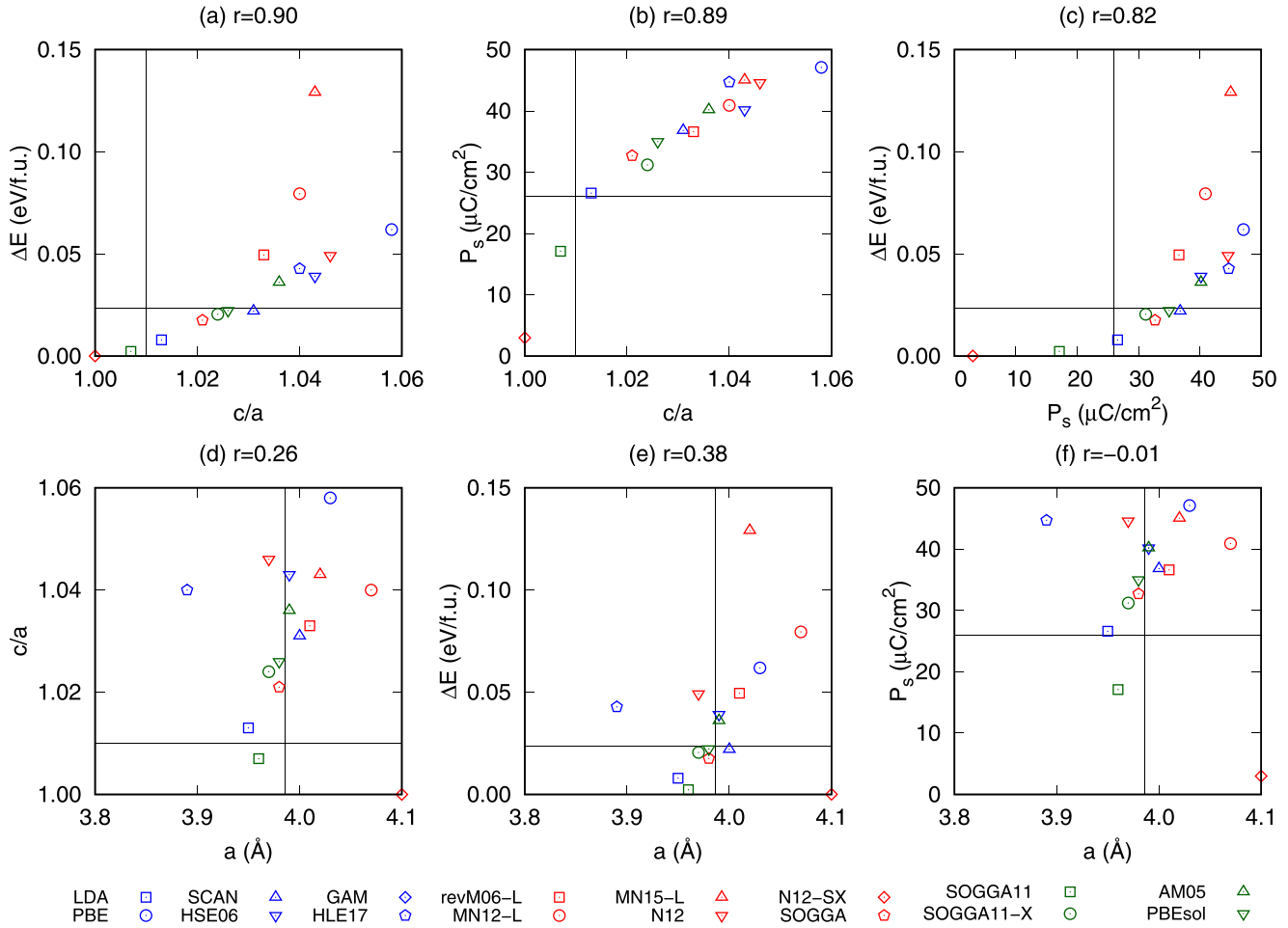
FIG. 3. Correlation plots for BTO. The correlation coefficient *r* is given above each graph. Experimental data are taken from Refs. [1], [2], [50], and [52]. Note that the GAM data are outside of plotting range.

a percentage next to the property. Based on the error, we rank the functionals for each property and add the rank to the tables next to the associated property.

Figure 2 presents the computational data for the energy and polarization evolution along the distortion path from cubic to tetragonal phase for BTO and PTO, respectively. Figures 2(a) and 2(b) and Figs. 2(d) and 2(e) show the potential well profiles, while Figs. 2(c) and 2(f) show the polarizations. For some of the functionals (PBE, HLE17, N12, GAM, SOGGA11-X, and AM05), we found that the cubic phase is a local minimum for PTO along the distortion path. For the HLE17, we investigated this by carrying out additional simulations where the search of the tetragonal phase was initiated by distorting the cubic structure along the eigenvector of an unstable phonon. Such relaxation yielded a different tetragonal phase which is only 31 meV/f.u. higher in energy than the original one but is structurally quite different. We presently attribute the issue of multiple minima for the HLE17 functional to the shortcomings of the functional itself. In this case, we use the lowest-energy structure for further analysis. We also note that the cohesive energies obtained with the GAM, MN12-L, and N12-SX for BTO and PTO and with the N12 for PTO are positive, which we attribute to the implementation. Figure 2 reveals that a deeper well is associated with larger spontaneous polarization. To

quantify this, we computed the correlation coefficient [57] $r_{xy} = \frac{\sum_i^n (x_i - \bar{x})(y_i - \bar{y})}{\sqrt{\sum_i^n (x_i - \bar{x})^2 \sum_i^n (y_i - \bar{y})^2}}$ between ΔE and P_s. In the expression, n is the sample size, x_i and y_i are the sample points, and $\bar{x}$ and $\bar{y}$ are the mean values. In addition, we computed the rest of the correlation coefficients associated with the set of four parameters: a_c, c/a, ΔE, and P_s. The dependencies are shown in Figs. 3 and 4. The correlation coefficients are shown above the panels. We find strong correlations between ΔE, c/a, and P_s predictions, indicating that the functional indeed defines how well the ferroelectric properties are captured. The correlation between P_c and c/a was also found in Ref. [12] for other functionals. At the same time, we find only weak correlation with the cubic lattice constant. Along the correlation lines, the functionals closest to the targets are the LDA, SOGGA, and SOGGA11-X for BTO and the PBEsol, SOGGA, and MN12-L for PTO.

To further assess the performance of functionals in describing a_c, P_s, c/a, E_g, and ΔE, we rank them using two approaches. In the first approach, each functional is ranked 1 through 16 in each category. The category here is defined by the respective property, such that we have five categories in total. The rank is determined by sorting the functionals from the lowest percentage error to the highest. Then, for a given functional, the rank is averaged over the four most
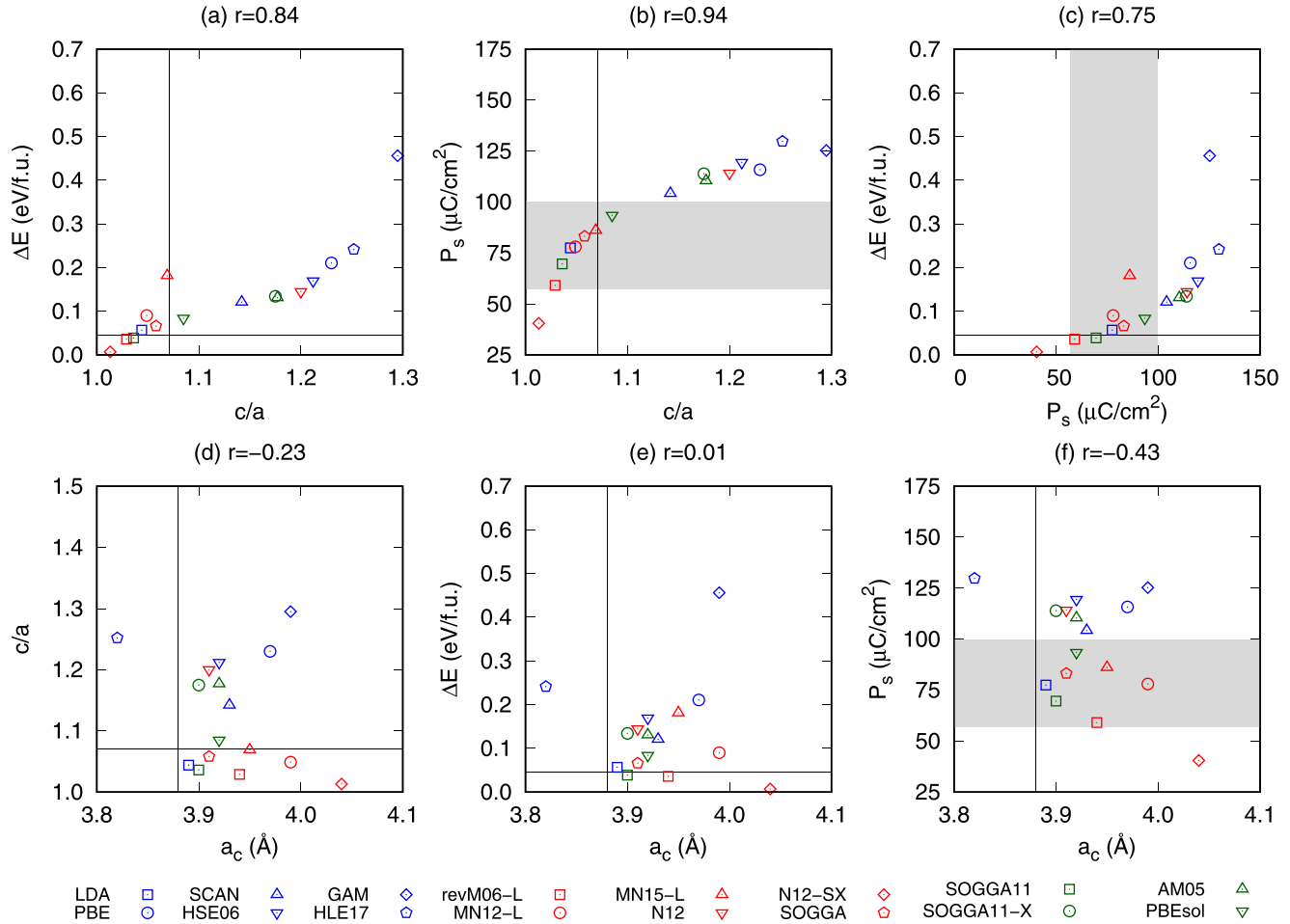
FIG. 4. Correlation plots for PTO. The correlation coefficient r is given above each graph. Experimental data are taken from Refs. [1], [2], [37], and [38].

relevant categories (a_c, P_s, c/a, ΔE), and the functionals are sorted by the average value and assigned an overall rank that is reported in the last column in Tables II and III. The second approach to ranking is more quantitative. For each category, we compute the relative error as $|e/e_{max}|$, where e_{max} is the largest error in the given category. The relative errors are reported in Tables IV and V. Next, the relative error is averaged over the four most relevant categories (a_c, P_s, c/a, ΔE) and reported in the last column in Tables IV and V. We note that the CPU time increases going up Jacob's Ladder. Roughly, the LDA and GGA exhibit comparable CPU times, which increase about three times as we move to the meta-GGA/NGA functionals. Hybrid functionals can be up to two orders of magnitude higher in computational cost.

V. DISCUSSION

We begin the discussion by acknowledging that, perhaps, the biggest challenge in assessing the performance of exchange-correlation functionals on ferroelectrics is the shortage of reliable benchmarks. The properties that are straightforward to obtain in computations, such as 0 K cohesive energies, polarization, and structural parameters cannot be directly compared with experiment. For example, the cohesive energies of the different phases, or even the difference in

their energies, are not directly available from experiment. The structural and electric properties are available at significantly higher temperatures and oftentimes exhibit variations.

TABLE IV. Relative errors for properties of BTO computed as $\Xi = |e/e_{max}|$, where e is the percentage error for the specific functional and e_{max} is the largest percentage error in the category.

	Ξ_{a_c}	$\Xi_{c/a}$	Ξ_{P_s}	$\Xi_{\Delta E}$	$\langle \Xi \rangle$
PBEsol	0.026	0.113	0.198	0.007	0.086
SOGGA	0.095	0.081	0.148	0.034	0.089
SOGGA11-X	0.155	0.100	0.115	0.017	0.097
LDA	0.310	0.021	0.012	0.089	0.108
SCAN	0.129	0.149	0.239	0.009	0.131
SOGGA11	0.233	0.021	0.197	0.121	0.143
AM05	0.017	0.186	0.313	0.072	0.147
HSE06	0.060	0.232	0.314	0.089	0.174
MN12-L	0.233	0.161	0.235	0.149	0.194
N12	0.103	0.257	0.412	0.147	0.230
PBE	0.397	0.336	0.467	0.220	0.355
MN15-L	0.681	0.214	0.330	0.320	0.386
revM06-L	0.293	0.235	0.421	0.604	0.388
HLE17	0.862	0.214	0.414	0.111	0.400
N12-SX	1.000	0.069	0.508	0.134	0.428
GAM	0.595	1.000	1.000	1.000	0.899

TABLE V. Relative errors for properties of PTO computed as $\Xi = |e/e_{\max}|$, where e is the percentage error for the specific functional and $e_{\max}$ is the largest percentage error in the category.

	Ξ_{a_c}	$\Xi_{c/a}$	Ξ_{P_s}	$\Xi_{\Delta E}$	$\langle \Xi \rangle$
LDA	0.049	0.127	0.046	0.027	0.063
SOGGA11	0.104	0.164	0.099	0.016	0.096
SOGGA	0.195	0.062	0.150	0.051	0.114
PBEsol	0.250	0.065	0.338	0.094	0.187
MN12-L	0.373	0.197	0.290	0.023	0.221
MN15-L	0.684	0.101	0.054	0.108	0.237
revM06-L	0.415	0.009	0.202	0.331	0.239
SCAN	0.324	0.333	0.533	0.184	0.343
SOGGA11-X	0.122	0.484	0.709	0.216	0.383
AM05	0.269	0.494	0.646	0.208	0.404
N12	0.189	0.605	0.716	0.242	0.438
N12-SX	1.000	0.269	0.630	0.094	0.498
HSE06	0.250	0.659	0.812	0.302	0.506
PBE	0.538	0.745	0.745	0.402	0.607
HLE17	0.348	0.845	1.000	0.477	0.668
GAM	0.690	1.000	0.917	1.000	0.902

Therefore, the assessment of performance can only be done with respect to some chosen set of metrics. In this study, we chose experimental data from the literature to serve as these benchmarks. A valuable finding of the present study is the presence of a strong correlation between the tetragonality, the spontaneous polarization, and the energy difference between the cubic and the tetragonal phases predicted by different functionals. Thanks to the correlation, it is possible to identify the best-performing functionals by their positions on the correlation line with respect to the target values. In our case Figs. 3 and 4 predict the best performers for BTO to be the LDA, PBEsol, SOGGA, and SOGGA11-X and those for PTO to be the LDA, PBEsol, SOGGA, and SOGGA11. The same conclusions are supported by the rankings of the functionals in Tables II–V, where the aforementioned functionals occupy the top positions. The top performers are marked by asterisks in Fig. 1. In the figures we can see that the functionals that perform well for both materials are the PBEsol, SOGGA, and LDA.

Our data, however, imply that the performances of functionals vary from one material to another as is evident from inspection of the correlation data in Figs. 3 and 4, where we find that the relative position of the functional on the curve depends on the material. For example, the revMO6-L overestimates properties for BTO and underestimates them for PTO. While this is somewhat discouraging, the availability of a range of functionals (like the Minnesota suite) could mitigate the problem. Indeed, the computations carried out in this project are inexpensive and could be done for any ferroelectric to produce correlation graphs and rankings. The top-performing functional(s) then can be used for further investigation. We recall that one of our motivations for this study was to determine the best functionals to be used for the parametrization of force fields and effective Hamiltonians for ferroelectrics [7,9,58–60]. While there seems to be no unique answer to this question, our study proposes an efficient recipe for the selection of the best functional. Moreover, the study

demonstrates that most of the functionals investigated here produce reasonable predictions and, therefore, can be used for such preliminary investigation. The exclusions here are the GAM functional from the Minnesota suite, which produces consistently poor predictions, and the hybrid functionals, which do not offer a significant improvement that could justify the computational cost. We also comment that among the Minnesota functionals, the SOGGA and SOGGA11 emerge as strong competitors to the LDA in predicting ΔE, P_s, and c/a for ferroelectrics. As far as the classical potentials parametrized from DFT are concerned, one critical issue is their inability to accurately predict the Curie temperature, with the LDA significantly underestimating the T_C and the GGA significantly overestimating it. Our data reveal that the predictions of many of the functionals fall between these two [see Figs. 2(a) and 2(b) for BTO and Figs. 2(d) and 2(e) for PTO] and, therefore, are likely to produce more accurate force fields.

For the bandgap predictions (see Tables II and III), we find that the hybrid functionals perform the best, with the exception of the SOGGA11-X. For BTO, we find that the MN15-L and MN12-L give surprisingly good predictions.

Interestingly, our findings suggest that moving up Jacob's Ladder does not guarantee an improvement in predictions. One of the reasons is, once again, the absence of absolute metrics for comparison. The other is that ferroelectricity is affected significantly by the nature of the bonding. As the exchange-correlation functional has a different effect on different types of bonding, it is not surprising that upward movement along Jacob's Ladder can produce different effects on different ferroelectrics. For example, in $BaTiO_3$ the distortion is dominated by the motion of Ti (B site), while in $PbTiO_3$ it is dominated by the Pb (A site). In the former case, it is primarily driven by the hybridization between O-$2p$ and Ti-$3d$ orbitals, while in the latter case, the hybridization between the stereochemically active lone pair on Pb and O-$2p$ electrons plays an important role. An excellent discussion of the physics of capturing bonding in ferroelectrics by different functionals is available in Ref. [1]. Following the argument presented in that work, we expect an improvement in description *across* the diversely bonded ferroelectrics rather than for each individual one as we move up Jacob's Ladder. Indeed, it was found that the SCAN improves on the LDA and GGA predictions for diversely bonded ferroelectrics [1].

VI. CONCLUSIONS

In this study, we assessed the performance of the recently introduced Minnesota functionals in comparison to the traditional ones (LDA and PBE) and some of the newer ones (AM05 and PBEsol) on the prototypical ferroelectrics BTO and PTO. We looked at the structural, electric, and energetic properties that are most critical for parametrization of classical force fields and Hamiltonians. We found that the predictions for ΔE, c/a, and P_s exhibit a strong correlation with one another between different functionals while showing no correlation with a_c. However, even for the properties that exhibit correlation, the relative position of the functional prediction along the correlation line is material dependent, suggesting that the performance of functionals is also material

dependent. Two ways to rank the functional performance against given benchmarks are suggested. We note that, unfortunately, there exists a shortage of reliable benchmarks for ferroelectric properties, which makes ranking dependent on the chosen set of benchmarks. Within the chosen benchmarks, 16 investigated functionals have been ranked using both methods. From the ranking, we once again found that the performance of the functional is material dependent. Because we found no "winner" among the chosen functionals, we propose that the performance of the functionals could be assessed prior to their use for predictions. In particular, the calculations and analysis carried out in this study are inexpensive (except for the hybrid functionals) and can be used to "screen" functionals prior to their employment. The value of the Minnesota functionals for such screening is that they significantly expand the space of exchange-correlation functionals suitable for ferroelectrics and, in many cases, bridge the LDA and PBE predictions, which are known to be on the far ends of the spectrum. Many of the tested functionals perform well on ferroelectrics, with predictions falling between the LDA and the PBE values.

ACKNOWLEDGMENTS

APPENDIX: ACRONYMS FOR EXCHANGE-CORRELATION FUNCTIONALS

TABLE VI. Acronyms for exchange-correlation functionals.

Functional	Full name
LDA	Local density approximation
PBE	Perdew-Burke-Ernzerhof GGA
PBEsol	PBE for solids
AM05	Armiento-Mattsson 2005
B1WC	Hybrid exchange-correlation functional of Bilc *et al.* [8]
B1WC(PP)	B1WC using pseudopotentials
SCAN	Strongly constrained and appropriately normed
HSE06	Heyd-Scuseria-Ernzerhofhybrid functional 2006
HSEsol	HSE for solids
TM	Tao-Mo meta-GGA
TPSS	Tao-Perdew-Staroverov-Scuseria meta-GGA
TPSS+U	TPSS with local correlation potential
GAM	Gradient approximation for molecules
HLE17	High Local Exchange 2017
M06-L	Minnesota 2006 local functional
revM06-L	Revised M06-L
MN12-L	Meta-NGA parameterized exchange-correlation functional 2012
MN15-L	Meta-NGA parameterized exchange-correlation functional 2015
N12	NGA parameterized exchange-correlation functional 2012
N12-SX	N12 with short-range Hartree-Fock exchanges
SOGGA	Second-order generalized gradient approximation
SOGGA11	Second-order generalized gradient approximation 2011
SOGGA11-X	Global hybrid form of SOGGA11

[1] Y. Zhang, J. Sun, J. P. Perdew, and X. Wu, Phys. Rev. B **96**, 035143 (2017).

[2] J. Sun, R. C. Remsing, Y. Zhang, Z. Sun, A. Ruzsinszky, H. Peng, Z. Yang, A. Paul, U. Waghmare, X. Wu, M. L. Klein, and J. P. Perdew, Nat. Chem. **8**, 831 (2016).

[3] R. D. King-Smith and D. Vanderbilt, Phys. Rev. B **49**, 5828 (1994).

[4] T. Hashimoto, T. Nishimatsu, H. Mizuseki, Y. Kawazoe, A. Sasaki, and Y. Ikeda, Jpn. J. Appl. Phys. **43**, 67851 (2004).

[5] Z. Wu and R. E. Cohen, Phys. Rev. B **73**, 235116 (2006).

[6] Z. Wu, R. E. Cohen, and D. J. Singh, Phys. Rev. B **70**, 104112 (2004).

[7] T. Nishimatsu, M. Iwamoto, Y. Kawazoe, and U. V. Waghmare, Phys. Rev. B **82**, 134106 (2010).

[8] D. I. Bilc, R. Orlando, R. Shaltaf, G.-M. Rignanese, J. Íñiguez, and P. Ghosez, Phys. Rev. B **77**, 165107 (2008).

[9] A. Paul, J. Sun, J. P. Perdew, and U. V. Waghmare, Phys. Rev. B **95**, 054111 (2017).

[10] J. Sun, A. Ruzsinszky, and J. P. Perdew, Phys. Rev. Lett. **115**, 036402 (2015).

[11] S. F. Yuk, K. C. Pitike, S. M. Nakhmanson, M. Eisenbach, Y. W. Li, and V. R. Cooper, Sci. Rep. **7**, 43482 (2017).

[12] Y. Watanabe, J. Chem. Phys. **148**, 194702 (2018).

[13] S. Duanmu, K. Luo, X. He, and D. G. Truhlar, Mn-vfm, version 2019-a; https://comp.chem.umn.edu/mn-vfm/ (2019).

[14] G. Kresse and J. Hafner, Phys. Rev. B **47**, 558 (1993).

[15] G. Kresse and J. Furthmuller, Comput. Mater. Sci. **6**, 15 (1996).

[16] G. Kresse and J. Furthmüller, Phys. Rev. B **54**, 11169 (1996).

[17] G. Kresse and D. Joubert, Phys. Rev. B **59**, 1758 (1999).

[18] Y. Zhao and D. G. Truhlar, J. Chem. Phys. **128**, 184109 (2008).

[19] Y. Peperstraete, E. Amzallag, R. Tétot, and P. Roy, J. Phys.: Condens. Matter **30**, 215702 (2018).

[20] Y. Mo, H. Tang, A. Bansil, and J. Tao, AIP Adv. **8**, 095209 (2018).

[21] N. Mardirossian and M. Head-Gordon, Mol. Phys. **115**, 2315 (2017).

[22] A. V. Krukau, O. A. Vydrov, A. F. Izmaylov, and G. E. Scuseria, J. Chem. Phys. **125**, 224106 (2006).

[23] J. Heyd, G. E. Scuseria, and M. Ernzerhof, J. Chem. Phys. **118**, 8207 (2003).

[24] J. Paier, M. Marsman, K. Hummer, G. Kresse, I. C. Gerber, and J. G. Ángyán, J. Chem. Phys. **124**, 154709 (2006).

[25] R. Peverati, Y. Zhao, and D. G. Truhlar, J. Phys. Chem. Lett. **2**, 1991 (2011).

[26] R. Peverati and D. G. Truhlar, J. Chem. Theory Comput. **8**, 2310 (2012).

[27] H. S. Yu, W. Zhang, P. Verma, X. He, and D. G. Truhlar, Phys. Chem. Chem. Phys. **17**, 12146 (2015).

[28] R. Peverati and D. G. Truhlar, Phys. Chem. Chem. Phys. **14**, 13171 (2012).

[29] H. S. Yu, X. He, and D. G. Truhlar, J. Chem. Theory Comput. **12**, 1280 (2016).

[30] P. Verma and D. G. Truhlar, J. Phys. Chem. C **121**, 7144 (2017).

[31] I. Choudhuri and D. G. Truhlar, J. Phys. Chem. C **123**, 17416 (2019).

[32] Y. Wang, X. Jin, H. S. Yu, D. G. Truhlar, and X. He, Proc. Natl. Acad. Sci. U.S.A. **114**, 8487 (2017).

[33] R. Peverati and D. G. Truhlar, J. Chem. Phys. **135**, 191102 (2011).

[34] R. Peverati and D. G. Truhlar, Phys. Chem. Chem. Phys. **14**, 16187 (2012).

[35] P. Hohenberg and W. Kohn, Phys. Rev. **136**, B864 (1964).

[36] W. Kohn and L. J. Sham, Phys. Rev. **140**, A1133 (1965).

[37] J. P. Perdew, K. Burke, and Y. Wang, Phys. Rev. B **54**, 16533 (1996).

[38] J. P. Perdew, K. Burke, and M. Ernzerhof, Phys. Rev. Lett. **77**, 3865 (1996).

[39] J. P. Perdew, A. Ruzsinszky, G. I. Csonka, O. A. Vydrov, G. E. Scuseria, L. A. Constantin, X. Zhou, and K. Burke, Phys. Rev. Lett. **100**, 136406 (2008).

[40] W. A. Al-Saidi and A. M. Rappe, Phys. Rev. B **82**, 155304 (2010).

[41] M. C. Kim, S. G. Lee, C. Joh, and H. S. Seo, Trans. Electr. Electron. Mater. **17**, 29 (2016).

[42] R. Armiento and A. E. Mattsson, Phys. Rev. B **72**, 085108 (2005).

[43] A. E. Mattsson and R. Armiento, Phys. Rev. B **79**, 155101 (2009).

[44] K. Persson, Materials Data on $BaHfO_3$ (SG:221) by Materials Project; https://www.osti.gov/dataexplorer/biblio/dataset/1317346 (2014).

[45] K. Persson, Materials Data on $BaHfO_3$ (SG:99) by Materials Project; https://www.osti.gov/dataexplorer/biblio/dataset/1189315 (2014).

[46] K. Lejaeghere, G. Bihlmayer, T. Björkman, P. Blaha, S. Blügel, V. Blum, D. Caliste, I. E. Castelli, S. J. Clark, A. Dal Corso, S. de Gironcoli, T. Deutsch, J. K. Dewhurst, I. Di Marco, C. Draxl, M. Dułak, O. Eriksson, J. A. Flores-Livas, K. F. Garrity, L. Genovese, P. Giannozzi, M. Giantomassi, S. Goedecker, X. Gonze, O. Grånäs, E. K. U. Gross, A. Gulans, F. Gygi, D. R. Hamann, P. J. Hasnip, N. A. W. Holzwarth, D. Iuşan, D. B. Jochym, F. Jollet, D. Jones, G. Kresse, K. Koepernik, E. Küçükbenli, Y. O. Kvashnin, I. L. M. Locht, S. Lubeck, M. Marsman, N. Marzari, U. Nitzsche, L. Nordström, T. Ozaki, L. Paulatto, C. J. Pickard, W. Poelmans, M. I. J. Probert, K. Refson, M. Richter, G.-M. Rignanese, S. Saha, M. Scheffler, M. Schlipf, K. Schwarz, S. Sharma, F. Tavazza, P. Thunström, A. Tkatchenko, M. Torrent, D. Vanderbilt, M. J. van Setten, V. Van Speybroeck, J. M. Wills, J. R. Yates, G.-X. Zhang, and S. Cottenier, Science **351**, aad3000 (2016).

[47] H. T. Stokes, D. M. Hatch, and B. J. Campbell, ISODISTORT [stokes.byu.edu/iso/isodistort.php] and ISOTROPY [https://stokes.byu.edu/iso/isotropy.php] Software Suites.

[48] B. J. Campbell, H. T. Stokes, D. E. Tanner, and D. M. Hatch, J. Appl. Crystallogr. **39**, 607 (2006).

[49] V. Wang, N. Xu, J. Liu, G. Tang, and W. Geng, arXiv:1908.08269.

[50] K. M. Rabe, M. Dawber, C. Lichtensteiger, C. H. Ahn, and J.-M. Triscone, Modern physics of ferroelectrics: Essential background, in *Physics of Ferroelectrics: A Modern Perspective* (Springer, Berlin, 2007), pp. 1–30.

[51] G. Shirane, H. Danner, and R. Pepinsky, Phys. Rev. **105**, 856 (1957).

[52] H. H. Wieder, Phys. Rev. **99**, 1161 (1955).

[53] S. H. Wemple, Phys. Rev. B **2**, 2679 (1970).

[54] S. A. Mabud and A. M. Glazer, J. Appl. Crystallogr. **12**, 49 (1979).

[55] V. Zametin, Phys. Status Solidi B **124**, 625 (1984).

[56] K. Carl, Ferroelectrics **9**, 23 (1975).

[57] S. M. Ross, *Introductory Statistics* (Elsevier Science & Technology, San Diego, CA, 2010).

[58] W. Zhong, D. Vanderbilt, and K. M. Rabe, Phys. Rev. Lett. **73**, 1861 (1994).

[59] B. K. Mani, C.-M. Chang, and I. Ponomareva, Phys. Rev. B **88**, 064306 (2013).

[60] B. K. Mani, S. Lisenkov, and I. Ponomareva, Phys. Rev. B **91**, 134112 (2015).